Alexandria Engineering Journal 78 (2023) 584–591

Contents lists available at ScienceDirect

Alexandria Engineering Journal

journal homepage: www.elsevier.com/locate/aej

Original Article

Ka-band flat panel circularly polarized antenna array for LEO satellite communication systems

Woo-Hee Lim [a], Seong-Mo Moon [b], Han Lim Lee [a,*]

[a] School of Electrical and Electronics Engineering, Chung-Ang University, Seoul 06974, South Korea
[b] Satellite Payload Research Section, ETRI, Daejeon 34129, South Korea

ARTICLE INFO

Keywords:
Circularly-polarized antenna array
Flat-panel antenna array
High-gain antenna
LEO satellite communications
mmWave antenna array

ABSTRACT

In this paper, a high gain circularly-polarized antenna array with a flat panel structure for low Earth orbit (LEO) satellite communication systems is proposed. This new CP structure can efficiently achieve high directivity and can easily be integrated with beamforming ICs (BFIC) when designing an antenna module, resulting in a good candidate for Ka-band satellite communications. Furthermore, the proposed FPAA can easily be extended to a larger scale array from a base unit in a 2 × 2 sub-array structure. Each sub-array is configured by four high-gain planar segmented antenna (PSA) elements with a sequentially rotating arrangement, where a single 4-channel BFIC can drive CP radiation. Unlike previously reported PSA elements that have limited CP performance, the proposed PSA-CP configuration adopts additional conductors and ground-via structures to further improve the CP gain, axial-ratio (AR), and cross-polarization (XPD) characteristics. To verify the performance of the proposed PSA-CP, a 2 × 2 left-hand circular polarization (LHCP) sub-array was fabricated at 28 GHz and tested with a BFIC. The measured 10-dB impedance and 3-dB AR bandwidths of the proposed 2 × 2 array were 13.92% and 12.5%, respectively. In addition, the measured peak gain was 15.2 dBic at 28.5 GHz with an XPD level of less than 15 dB.

1. Introduction

As high-speed communication networks based on low Earth orbit (LEO) satellites have been established, the congestion and overload on existing networks are expected to ease once a sufficient number of LEO satellites are launched on the desired orbits. The LEO satellite communications are considered to play an important role in maritime and mountainous terrain communications, where terrestrial communication services are limited. Furthermore, Ka-band satellite communications are becoming factors in satellite-to-satellite communication, next-generation mobile communication, and autonomous driving due to their high bandwidth and high data-rate capability. Thus, antenna technologies that can be efficiently adopted in Ka-band LEO satellite systems have been actively studied [1–2]. When designing Ka-band array antennas for satellite communications, integration of both the antenna elements and the beamforming ICs (BFIC) must be carefully considered in addition to the typical challenges, such as the increased number of array elements, power consumption, and cost. Referring to Fig. 1, a large-scale phased array is required to form a high-directivity antenna mounted on an LEO payload for both space-to-space and space-to-ground communications. Here, multi-channel radio frequency integrated circuits (RFICs) are required within the antenna module to drive the relative phase and amplitude balance for the massive number of antenna elements to generate the desired beams. Typically, 4-channel BFICs are required to pair with four antenna elements to produce circularly polarized (CP) patterns. To overcome the high propagation losses in the Ka-band, high-gain antenna elements that can be easily integrated with BFICs are required. Therefore, planar antenna structures are preferred for direct attachment on planar chip shapes using the conventional fabrication process.

Various high-gain antenna structures have been proposed to overcome high-band losses. For example, superstrate-based high-gain antennas have used extra air-gapped layers with conductive patterns above the main radiators to further improve the gain [3–7]. Although high gain could be achieved, some problems have resulted such as high costs, large size, design complexity considering the refractive index of the substrate, and the impact of the extra layers on surrounding parts. In addition, various lens antennas have been proposed to improve the radiation directivity [8–9], although the design and fabrication complexity increase due to performance variations, which depend on the shape, size,

* Corresponding author.
E-mail address: hanlimlee@cau.ac.kr (H.L. Lee).

https://doi.org/10.1016/j.aej.2023.07.081
Received 30 May 2023; Received in revised form 14 July 2023; Accepted 31 July 2023
Available online 5 August 2023

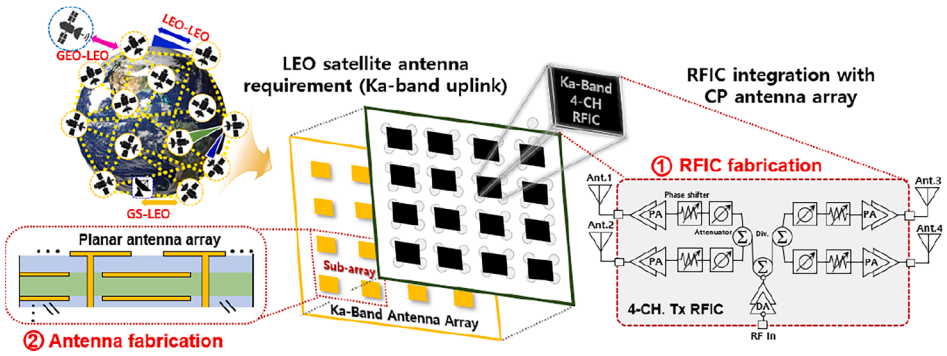

Fig. 1. Array Antenna requirement for next-generation LEO satellite communication using Ka-band uplink.

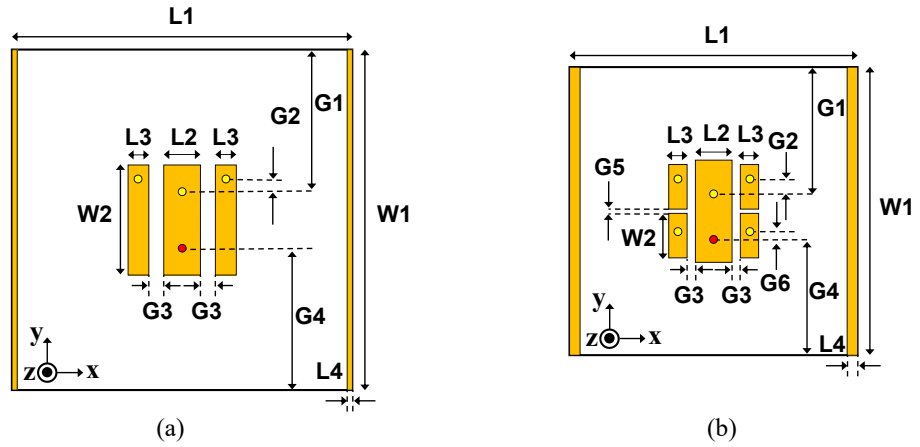

Fig. 2. Antenna configuration with (a) previously reported PSA [21] and (b) modified PSA.

and material of the lenses. Dielectric resonator antennas have also been proposed [10–15], although the antenna performance strongly depends on the size, shape, relative location within the feed network, and material of the resonators. Furthermore, high production costs, large profiles and sizes, and difficulty of fabrication are additional limitations. An antenna with a metallic cavity structure for gain enhancement has also been proposed [16–17]. However, integrating multiple chips in a single module, high volume, and weight (due to the metallic structure) are drawbacks. Finally, end-fire antennas (including director and dipole antenna structures) have been suggested as high-gain antennas [18–21]. However, when expanding two-dimensional arrays (including BFICs), the antenna volume efficiency is low and integration as a planar module is not feasible.

As mentioned previously, expansion to large-scale arrays is essential to implement sufficient communication performance, such as high data rates, low losses, and minimal mutual interferences. However, when designing planar modules with various ICs, the previously mentioned antennas are limited due to the high profile, costs, fabrication complexity, and structural issues. To overcome these problems, a high-gain antenna with a planar segmented patch (PSA) structure was recently proposed [22]. However, the performance of the PSA array was not analyzed and, more importantly, the CP orientation was not verified. In this paper, the direct application of PSAs for CP orientation is proved to be less effective compared to linear polarization (LP). Hence, a new PSA-CP antenna array is proposed for the first time based on a unit array of 2 × 2 with a sequential rotation in 90° and designed at Ka-band for LEO satellite communication uplinks. In addition, the proposed structure can achieve high CP gain with a wide 3-dB axial ratio (AR), cross-

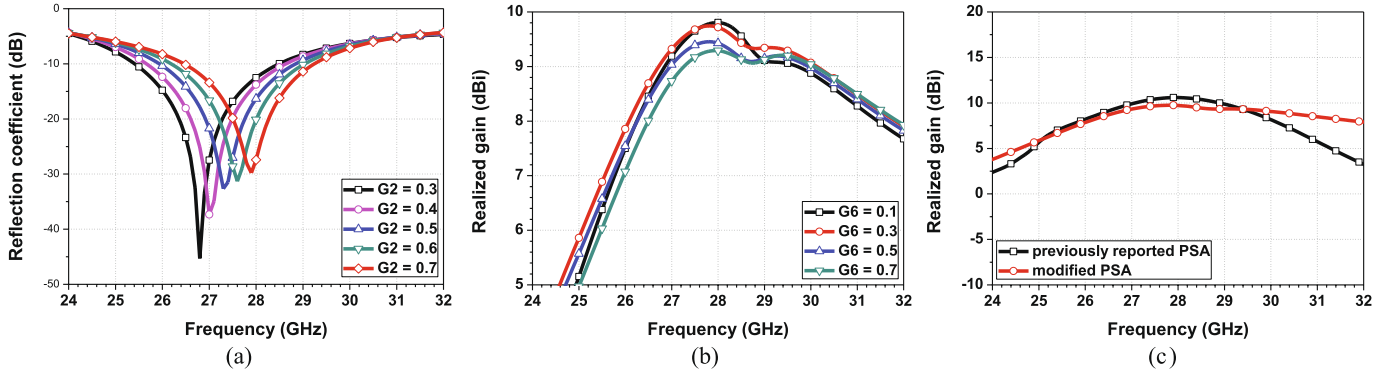

Fig. 3. Simulated (a) reflection coefficients according to G2 and (b) peak realized gain according to G6 of the modified PSA, and gain comparison with the previously reported PSA.

Table 1
Summary of the design parameters for conventional and modified PSAs.

Parameters: (mm)	Conventional	Modified
L1	13	11
L2	1.4	1.4
L3	0.8	0.7
L4	0.2	0.4
W1	13	11
W2	4.2	1.7
G1	5.4	5
G2	0.3	0.7
G3	0.5	0.25
G4	5.4	4.4
G5	–	0.2
G6	–	0.3

polarization suppression, and stable gain variation.

2. Design and analysis of the proposed antenna array

In previous research, high-gain antenna structures (known as PSAs) configured by multiple segmented conductors and shorting pins have been proposed, as displayed in Fig. 2 (a) [22]. The fundamental operation of a PSA is based on inducing multiple magnetic currents and enhancing radiating apertures to form a stronger magnetic field above the radiators. However, the conventional PSA has imbalances in the shorting pins concentrated at the opposite side of the excitation port, resulting in a high contribution of inductances from the side conductors to the antenna gain as the frequency increases. Thus, to minimize the effect of these inductances of the side conductors, the PSA is modified in this paper, as depicted in Fig. 2 (b). This newly proposed structure is optimized by adding more capacitive loading to compensate for the large inductances, where the inductances are distributed in parallel by segmenting more pieces of the shorted conductors. As a result, the modified PSA can improve the gain variation at high frequencies within the operation bandwidth. Furthermore, the required ground size to achieve the same gain as a conventional PSA can be reduced in the modified PSA structure.

Fig. 3 (a) and (b) display the parametric analyses for the reflection coefficient and peak realized gain for determining the shorting pin offset G2 and G6 in the modified PSA. The center frequency can be tuned first by setting the values of G2. Then, the peak gain in the operation band can be optimized with G6. Having optimized G2 and G6, the simulated 10-dB impedance bandwidth of the modified PSA is 10% with a center frequency at 28 GHz. Furthermore, the peak gain of the modified PSA is 9.7 dBi. Fig. 3 (c) displays a gain-flatness comparison of the conventional and modified PSAs, where the modified PSA exhibited less gain variation at high frequencies. The simulated gain variations of the conventional and modified PSAs were 3.15 and 1.51 dBi, respectively, within their 10-dB impedance bandwidths. The optimized parameters for the modified PSA are summarized in Table 1, including the conventional PSA as a reference.

Since CP must be used for satellite communications, the antenna elements are arranged with a 90° phase sequential rotation, as depicted in Fig. 4 (a), which includes a description of the design process for the proposed PSA-CP array. In Step 1, the four modified PSA elements are placed in a 90° sequential rotation to generate left-hand circular polarization (LHCP). First, the antenna spacing needs to be optimized, since the gain and side lobe level (SLL) must be considered simultaneously as well as the cross-polarization discrimination (XPD) level. The port-to-port distance with relatively high gain and XPD performance was optimized by a parametric analysis with G1, as displayed in Fig. 4 (b). Although an increase in antenna spacing can improve gain, SLL also increases, resulting in limited separation between the antenna elements. Thus, to further increase the gain of the CP orientation, an additional conductor in a cross shape was placed at the center of the array, as depicted in Step 2 in Fig. 4 (a). The ends of the cross-shaped conductor were shorted to ground to ensure axial ratio (AR) characteristics. The increased directivity with the center conductor can be observed in Fig. 4 (c), where the gain increased from 10.8 to 13.8 dBic. Furthermore, additional conductors were placed at the edges of the antenna to further

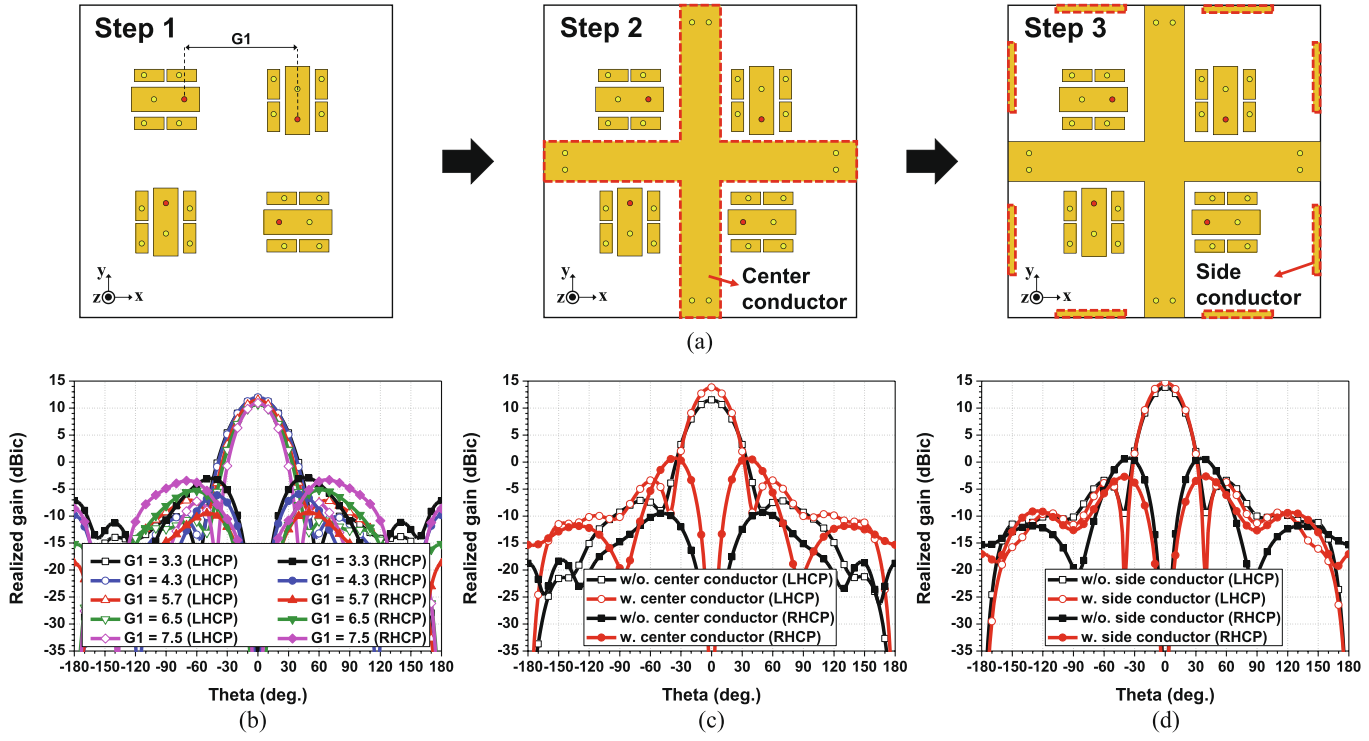

Fig. 4. Proposed PSA-CP configuration with (a) simplified design process and simulated results for realized gain according to (b) G1, (c) center conductor, and (d) side conductor.

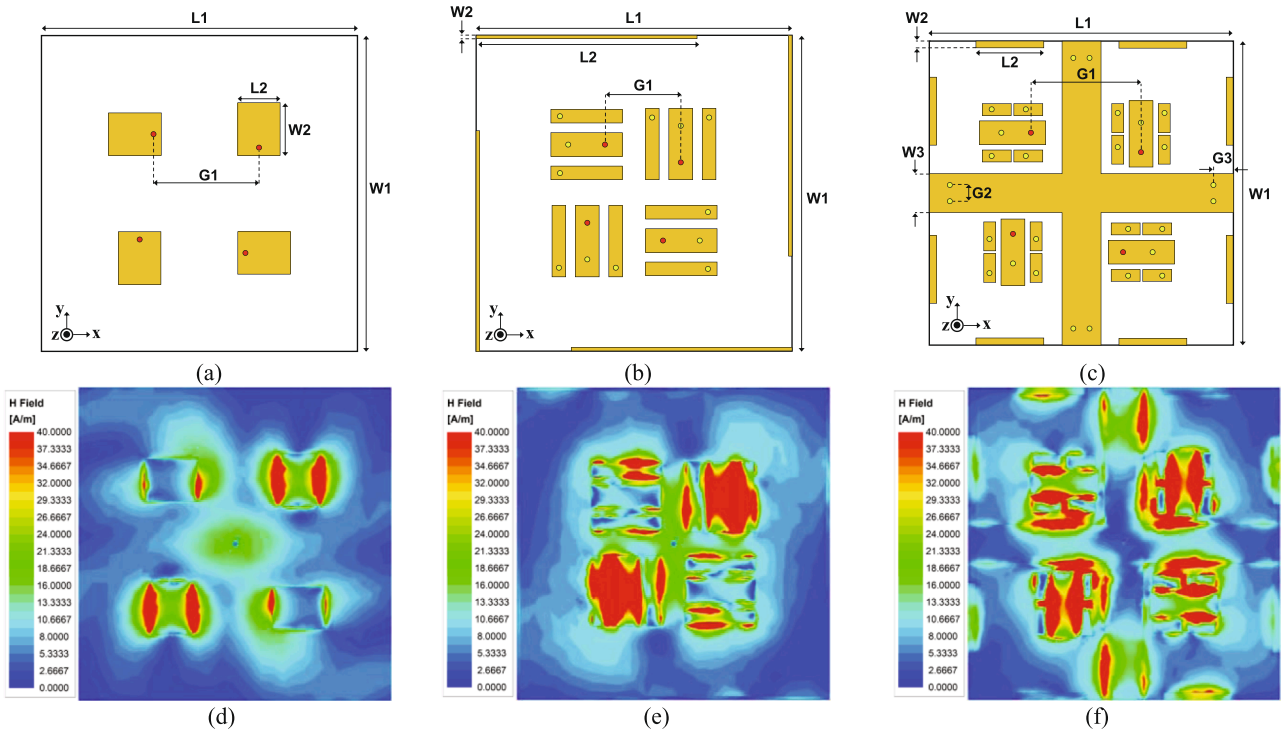

Fig. 5. 2 × 2 CP configurations with (a) the conventional patch (reference), (b) previously reported PSA (Type-A), and (c) proposed PSA-CP, and the 3-D EM simulated surface currents for (d) reference-CP, (b) Type-A-CP, and (c) proposed PSA-CP.

enhance the gain by focusing more field within the radiation aperture, as demonstrated in Step 3 in Fig. 4 (a). The simulated gain of the proposed PSA-CP in Step 3 exhibited an enhancement from 13.8 to 14.7 dBic, while the XPD level was suppressed from 13.1 to 17.3 dB, as displayed in Fig. 4 (d). Therefore, the addition of side and center conductors of the antenna improved the antenna gain by 3.9 dB within the same limited plane while mitigating XPD degradation. That is, the proposed PSA-CP exhibited both high directivity and XPD performances.

To clarify the enhanced gain performance of the proposed PSA-CP, 2 × 2 arrays with a conventional patch, the previously reported PSA, and the proposed-CP were designed and compared, as displayed in Fig. 5 (a), (b), and (c), respectively. The design parameters are summarized in Table 2, where conventional patch-based CP and the previously reported PSA-based CP antennas are denoted as the reference-CP and Type-A-CP to clearly distinguish them from the proposed PSA-CP antenna. In addition, Fig. 5 (d)–(f) displays the 3-D electromagnetic (EM) simulated surface currents for each reference, Type-A, and PSA-CP antenna, respectively. The proposed PSA-CP exhibited more surface current within the radiation aperture than the other CP antennas, resulting in improved gain characteristics.

Next, the radiation patterns (including cross-polarizations) for the reference-CP, Type-A-CP, and proposed PSA-CP antennas were simulated at 28 GHz, as presented in Fig. 6 (a), (b), and (c), respectively. The simulated peak realized gains of the reference-CP, Type-A-CP, and proposed PSA-CP antennas in both the xz and yz plane were 12.7, 12.2, and 14.7 dBic, respectively. As mentioned earlier in the paper, the previously reported PSA in a CP orientation did not exhibit gain enhancement compared to the conventional patch-based CP antenna. However, the proposed PSA-CP exhibited a gain enhancement of 2.5 dB compared to the Type-A-CP antenna. The simulated gains and ARs are presented in Fig. 6 (d)–(f), where the proposed PSA-CP exhibited excellent performance compared to the other structures.

Table 2
Summary of parameters in Fig. 3.

Parameters:(mm)	Reference-CP	Type-A-CP	ProposedPSA-CP
L1	18.6	18.6	17.9
L2	2.5	13	4
W1	18.6	18.6	17.9
W2	3.1	0.2	0.4
W3	–	–	2.2
G1	6.5	4.4	5.7
G2	–	–	1
G3	–	–	1.25

3. Fabrication and measurement

To verify the proposed PSA-CP antenna performance, a PSA-CP antenna was fabricated with a Taconic TLX-9 substrate having a relative permittivity of 2.5, a loss tangent of 0.019, and a thickness of 1.14 mm. Fig. 7 (a) displays the printed circuit board (PCB) layer information and Fig. 7 (b) presents the fabricated PSA-CP antenna. The conducting layer was printed with 1 oz copper and four SMPM RF connectors were used to measure the reflection coefficient for each element. The detailed geometric parameters of the fabricated PSA-CP antenna are summarized in Tables 1 and 2. The simulated and measured reflection coefficients are compared in Fig. 7 (c), exhibiting excellent agreement. The measured minimum 10-dB impedance bandwidth was 13.92 % with a center frequency of 28 GHz. Moreover, the measured isolations between each antenna element were always better than 15 dB within the 10-dB impedance bandwidth.

The proposed PSA-CP antenna was then integrated with a commercially available 4-ch beamforming IC (BFIC) (Anokiwave AWMF-0162), as displayed in Fig. 8 (a). The BFIC was configured by 6-bit phase shifters and 5-bit variable gain amplifiers, resulting in the phase and gain control

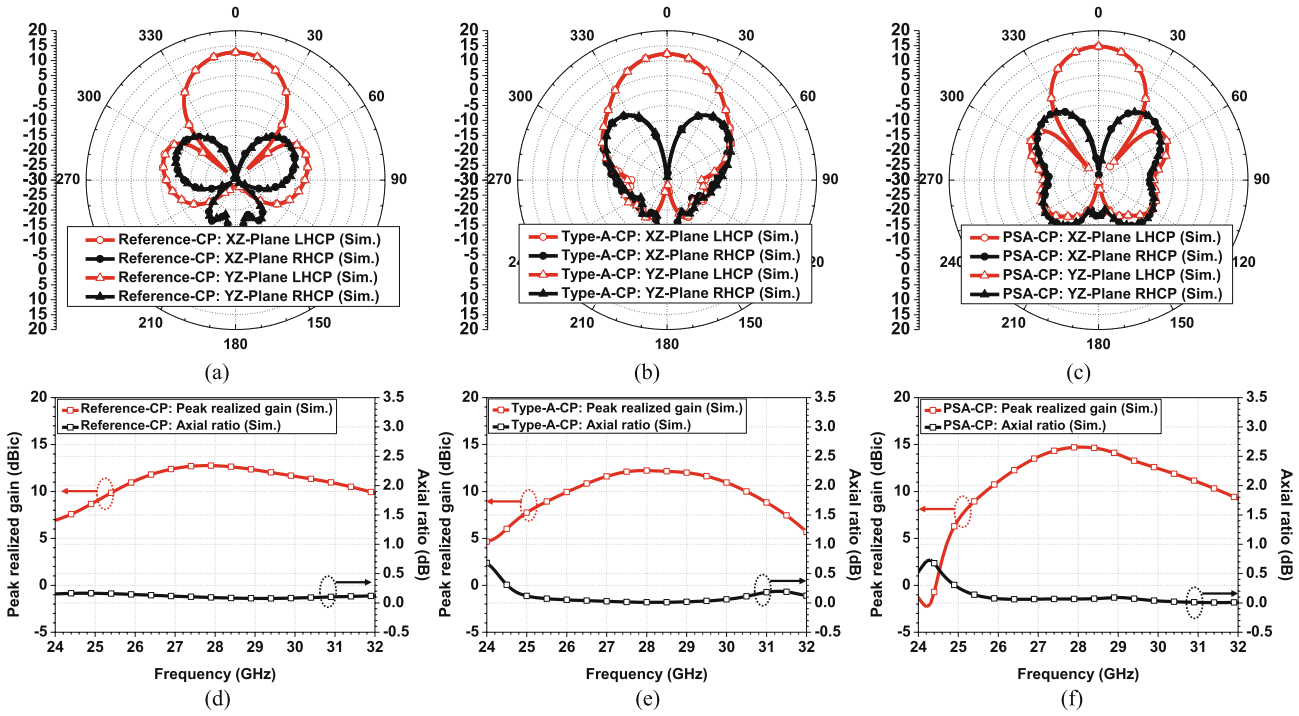

Fig. 6. Simulated radiation patterns at 28 GHz for (a) reference-CP, (b) Type-A-CP, and (c) proposed PSA-CP, and simulated gain and AR over frequencies for (d) reference-CP, (e) Type-A-CP, and (f) proposed PSA-CP.

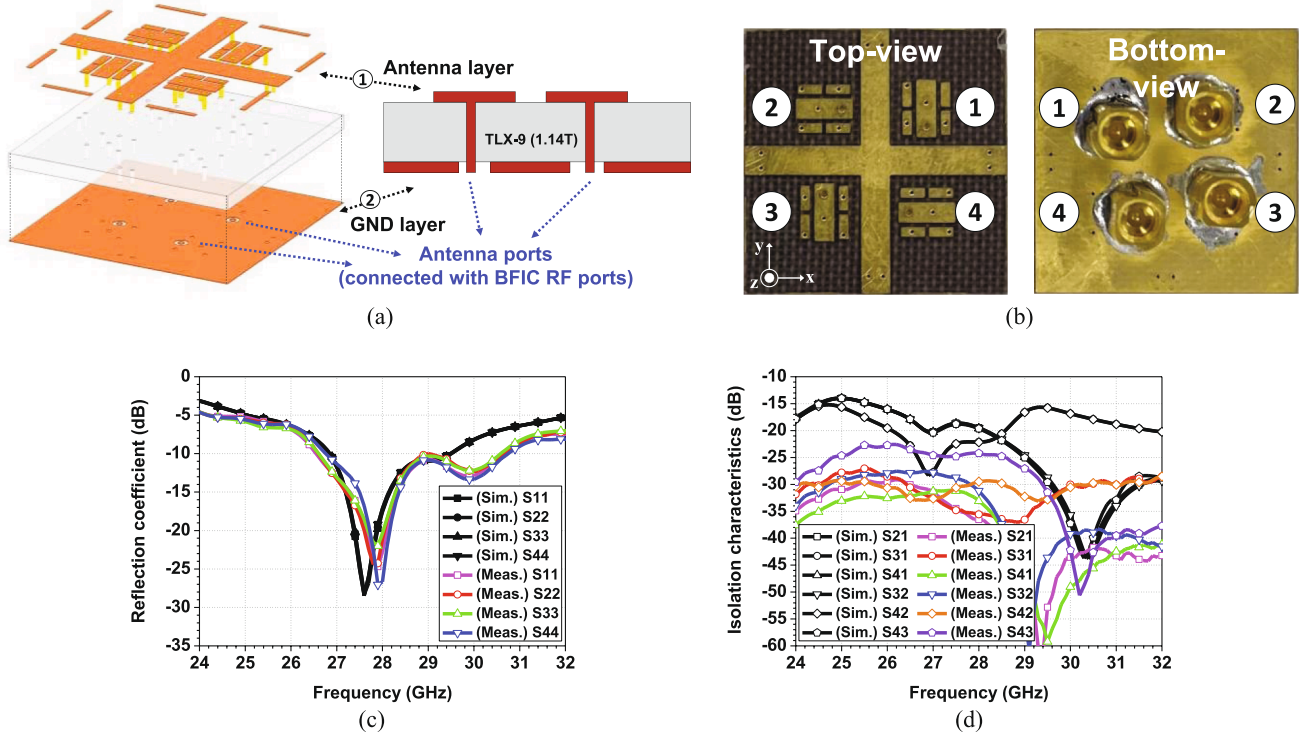

Fig. 7. Proposed PSA-CP antenna with (a) printed layer information, (b) fabrication photograph, (c) simulated and measured reflection coefficients, and (d) simulated and measured isolation for all elements.

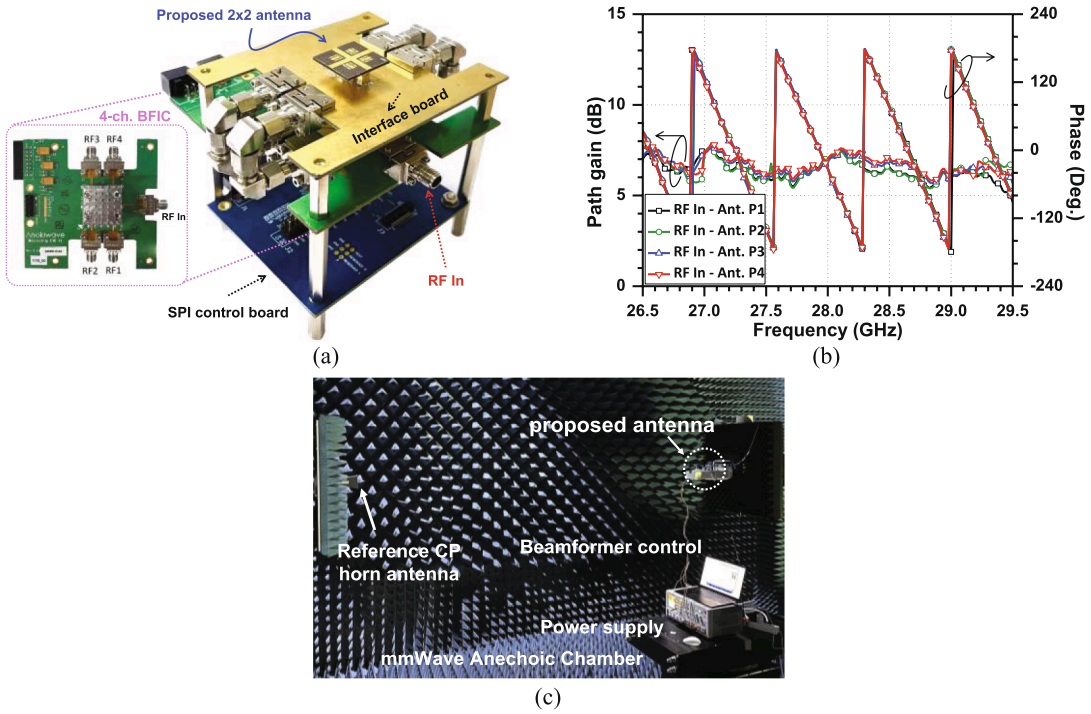

Fig. 8. Proposed PSA-CP antenna with (a) beamformer integration, (b) calibrated amplitudes and phases, and (b) measurement set-up.

resolutions of 5.6° and 0.5 dB, respectively. Although the BFIC specifications were provided from the manufacturer, the actual measurement showed discrepancy. Thus, the measured performances of the BFIC used for the proposed PSA-CP are summarized in Table 3. Then, each channel of the BFIC including the interface board was manually calibrated and then 90° phase shifts between the antenna elements were driven by the beamformer. The calibrated path amplitudes and phases including the connectors, adapters, and interface board losses of the beamformer are presented in Fig. 8 (b). Furthermore, Fig. 8 (c) displays the radiation pattern measurement set-up in a mmWave anechoic chamber.

The simulated and measured radiation patterns at different frequencies with the de-embedded beamformer gain are presented in Fig. 9. The measured peak gains of the proposed PSA-CP antenna in the xz and yz planes at 27 GHz were 13.1 and 12.8 dBic, respectively, as displayed in Fig. 9 (a)–(b). Furthermore, the measured half-power beamwidths (HPBW) in the xz and yz planes were 28° and 27°, respectively. In addition, the measured XPD levels were better than 10.3 dB. The measured peak gains of the proposed PSA-CP antenna in the xz and yz planes at 28 GHz were 14.7 and 14.7 dBic, respectively, as displayed in Fig. 9 (c)–(d). Moreover, the measured HPBW in the xz and yz planes were 27° and 27°, respectively. The measured XPD levels were better than 14.5 dB and the measured peak gains of the proposed PSA-CP antenna in the xz and yz planes at 29 GHz were 12.2 and 12.3 dBic, respectively, as displayed in Fig. 9 (e)–(f). The measured HPBW in the xz and yz planes were 26° and 26°, respectively, while the measured XPD levels were better than 13 dB. Fig. 9 (d) displays the measured peak gains and ARs over frequencies.

Finally, the proposed PSA-CP antennas were compared with other state-of-the-art mmWave high gain CP antennas, as presented in Table 4. To clarify the gain performance of the proposed antenna, the figure-of-merit was defined as the gain per total antenna volume (including the ground plane). Since the proposed PSA-CP was a planar structure, the highest FoM could be achieved, proving it is a good candidate for next-generation Ka-band satellite communications.

Table 3
Specification of the BFIC used for the proposed PSA-CP.

Specifications	Measured values
Operation band (GHz)	26.5—29.5
Tx output P1-dB (dBm)	6.3
Avg. Tx gain (dB)	19.1
Avg. Rx gain (dB)	18
Phase control resolution (°)	5.6 (6-bit)
Gain control resolution (dB)	0.5 (5-bit)
Supply voltage (V)	1.8

4. Conclusion

In this paper, a new planar CP antenna structure for next-generation Ka-band satellite communications was proposed. The proposed antenna was configured by 2 × 2 modified PSA elements and exhibited gain flatness compared to the previously reported PSA. The proposed PSA-CP antenna was optimized by adding extra conductors and shorting pins to further increase the gain and XPD levels while satisfying a good 3-dB AR bandwidth. The proposed PSA-CP antenna was fabricated with a Taconic PCB and integrated with a 4-ch BFIC. The PSA-CP antenna achieved a peak gain of 14.4 dBic at 28 GHz and the highest gain per antenna volume ratio compared to the other state-of-the-art mmWave CP antennas. For example, if a required antenna gain is 34 dBic, the required number of the conventional 2 × 2 patch-based sub-array having an antenna gain of 11 dBic is 256. This implies that the antenna elements are 1024 while the required number of BFICs is 256. On the other hand, the proposed 2 × 2 PSA-CP shows the maximum gain more than 14 dBic, resulting in the required numbers of antenna elements and BFICs being 512 and 128, respectively. Therefore, the total array size and the part numbers can be halved while maintaining the same EIRP by using the proposed antenna technique. Moreover, since the proposed PSA-CP antenna is based on a planar structure and can be easily integrated with BFICs, it can also be easily expanded to larger array scales and is an excellent candidate for large-scale phased array antennas in Ka-band satellite communications.

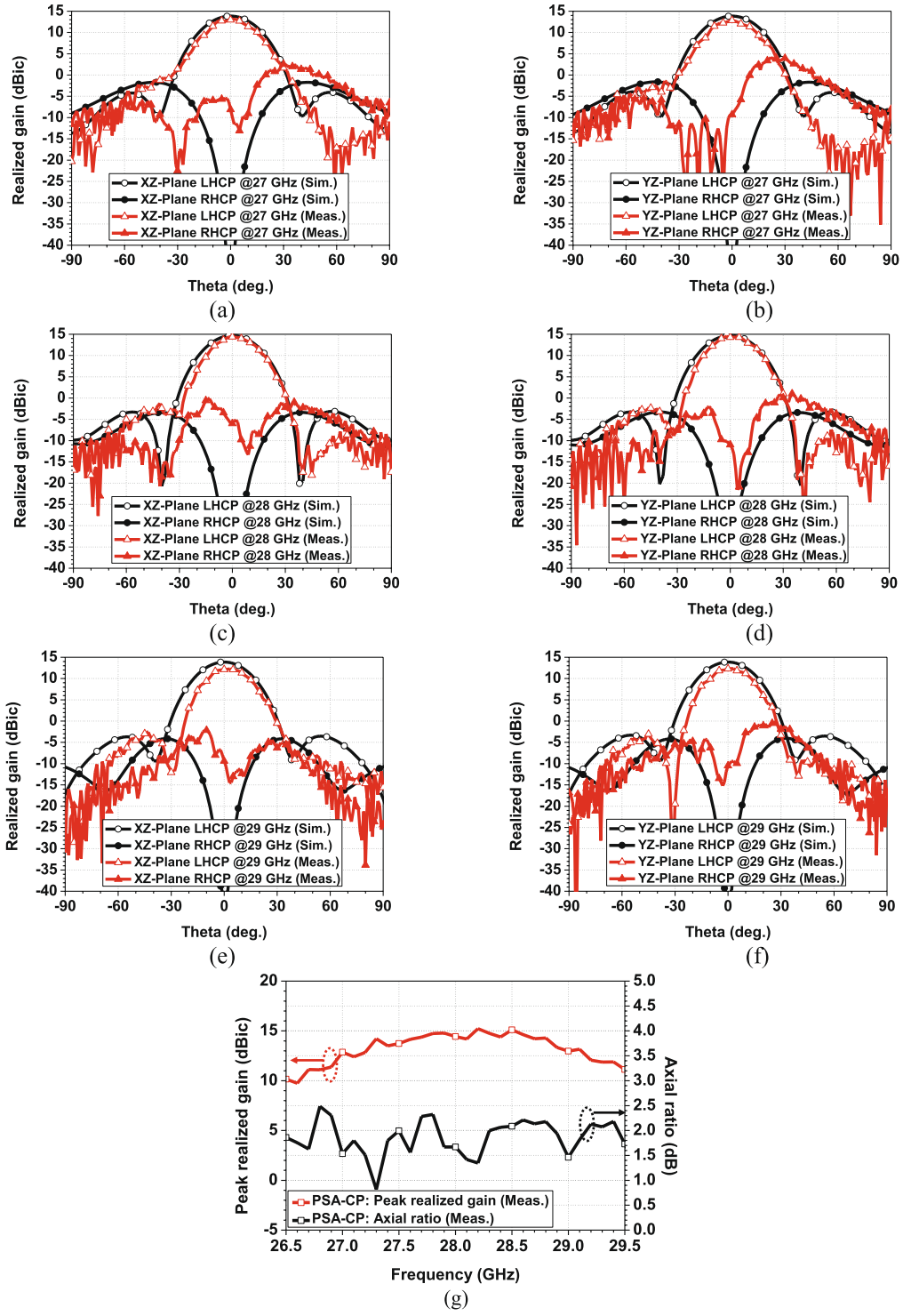

Fig. 9. Simulated and measured beam patterns in xz and yz planes for PSA-CP antenna at (a) 27 GHz, (b) 28 GHz, and (c) 29 GHz and (d) measured peak realized gain and axial ratio.

Table 4
Comparison of the state-of-the-art mmWave high gain antennas and arrays.

Ref.	Antennatopology	Total antenna volumewith ground plane (λ_0^3)	Center Freq. (GHz)	Impedance Bandwidth (%)	3-dB AR Bandwidth (%)	Peak gain (dBic)	FoM*(gain/λ_0^3)
[23]	FSS	34 × 34 × 1.27	30	14.3	14.6	31	0.02
[24]	Stacked dielectric resonator	0.96 × 1.26 × 0.27	30	12.8	4.1	8.2	25.11
[25]	Leaky-wave	10.22 × 2.98 × 0.03	31.9	40.6	40.6	12.5	13.68
[26]	Substrate integrated waveguide	6.53 × 5.93 × 0.21	28	6.07	4.64	13.52	1.66
[27]	Waveguide	8.5 × 8.5 × 7	30	13.3	13.3	26.87	0.05
This work	Planar	1.67 × 1.67 × 0.11	28	13.92	12.5	14.4	46.94

* FoM = antenna gain / total volume including ground plane.

Declaration of Competing Interest

The authors declare that they have no known competing financial interests or personal relationships that could have appeared to influence the work reported in this paper.

Acknowledgment

This research was supported in part by the Development of Civil Military Technology Project from the Institute of Civil Military Technology Cooperation (ICMTC) under Grant 21-CM-RA-02, and in part by the Institute for Information & Communications Technology Planning & Evaluation (IITP) grant funded by the Korean government (MSIT) (No.2019-0-00138, Development of Intelligent Radar Platform Technology for Smart Environments and No. 2018-0- 00190, Development of Core Technology for Satellite Payload).

References

[1] N.U.L. Hassan, C. Huang, C. Yuen, A. Ahmad, Y. Zhang, Dense small satellite networks for modern terrestrial communication systems: benefits, infrastructure, and technologies, IEEE Wirel. Commun. 27 (2000) 96–103.
[2] F.S. Prol, et al., Position, navigation, and timing (PNT) through low earth orbit (LEO) satellites: a survey on current status, challenges, and opportunities, IEEE Access 10 (2022) 83971–84002.
[3] L. Leszkowska, M. Rzymowski, K. Nyka, L. Kulas, High-gain compact circularly polarized X-band superstrate antenna for cubesat applications, IEEE Antennas Wirel. Propag. Lett. 20 (2021) 2090–2094.
[4] A.R. Vaidya, R.K. Gupta, S.K. Mishra, J. Mukherjee, Right-hand/left-hand circularly polarized high-gain antennas using partially reflective surfaces, IEEE Antennas Wirel. Propag. Lett. 13 (2014) 431–434.
[5] M. Abdollahvand, K. Forooraghi, J.A. Encinar, Z. Atlasbaf, E. Martinez-de-Rioja, A 20/30 GHz reflectarray backed by FSS for shared aperture Ku/Ka-band satellite communication antennas, IEEE Antennas Wirel. Propag. Lett. 19 (2020) 566–570.
[6] Z. Wu, L. Li, Y. Li, X. Chen, Metasurface superstrate antenna with wideband circular polarization for satellite communication application, IEEE Antennas Wirel. Propag. Lett. 15 (2016) 374–377.
[7] H.-J. Dong, Y.-B. Kim, J. Joung, H.L. Lee, High gain and low-profile stacked magneto-electric dipole antenna for phased array beamforming, IEEE Access 8 (2020) 180295–180304.
[8] Y. Cheng, Y. Dong, High-gain all-metal 3-D printed lens-horn antenna for millimeter-wave applications, IEEE Antennas Wirel. Propag. Lett. 22 (2023) 308–312.
[9] G.H. Lee, S. Kumar, H.C. Choi, K.W. Kim, Wideband high-gain double-sided dielectric lens integrated with a dual-bowtie antenna, IEEE Antennas Wirel. Propag. Lett. 20 (2021) 293–297.
[10] E. Baldazzi, et al., A high-gain dielectric resonator antenna with plastic-based conical horn for millimeter-wave applications, IEEE Antennas Wirel. Propag. Lett. 19 (2020) 949–953.
[11] L. Wang, et al., Stable high-gain linearly and circularly polarized dielectric resonator antennas based on multiple high-order modes, IEEE Trans. Antennas Propag. 70 (2022) 12270–12275.
[12] L. Zhong, J.-S. Hong, H.-C. Zhou, A novel pattern-reconfigurable cylindrical dielectric resonator antenna with enhanced gain, IEEE Antennas Wirel. Propag. Lett. 15 (2016) 1253–1256.
[13] W.-W. Yang, X.-Y. Dong, Y.-L. Li, J.-X. Chen, A self-packaged circularly polarized dielectric resonator antenna with wide bandwidth and high gain, IEEE Antennas Wirel. Propag. Lett. 17 (2018) 2188–2192.
[14] P.F. Hu, Y.M. Pan, X.Y. Zhang, S.Y. Zheng, A compact filtering dielectric resonator antenna with wide bandwidth and high gain, IEEE Trans. Antennas Propag. 64 (2016) 3645–3651.
[15] S. Varghese, P. Abdulla, A.M. Baby, J.P.M., High-gain dual-band waveguide-fed dielectric resonator antenna, IEEE Antennas Wirel. Propag. Lett. 21 (2022) 232–236.
[16] X. Li, J. Xiao, Z. Qi, H. Zhu, Broadband and high-gain SIW-fed antenna array for 5G applications, IEEE Access 6 (2018) 6282–56289.
[17] J. Zhu, C.-H. Chu, L. Deng, C. Zhang, Y. Yang, S. Li, mm-Wave high gain cavity-backed aperture-coupled patch antenna array, IEEE Access 6 (2018) 44050–44058.
[18] C. Mao, M. Khalily, P. Xiao, L. Zhang, R. Tafazolli, High-gain phased array antenna with endfire radiation for 26 GHz wide-beam-scanning applications, IEEE Trans. Antennas Propag. 69 (2021) 3015–3020.
[19] M. Xiao, A.K. Rashid, B. Liu, R. Fan, Q. Zhang, Design of high-gain single-layer endfire antenna using phase-reversed asymmetric spoof surface plasmon polaritons, IEEE Antennas Wirel. Propag. Lett. 22 (2023) 641–644.
[20] M. Heino, C. Icheln, J. Haarla, K. Haneda, PCB-based design of a beamsteerable array with high-gain antennas and a rotman lens at 28 GHz, IEEE Antennas Wirel. Propag. Lett. 19 (2020) 1754–1758.
[21] X.-F. Zhang, J. Fan, J.-X. Chen, High gain and high-efficiency millimeter-wave antenna based on spoof surface plasmon polaritons, IEEE Trans. Antennas Propag. 67 (2019) 687–691.
[22] J. Kim, H.L. Lee, High gain planar segmented antenna for mmWave phased array applications, IEEE Trans. Antennas Propag. 70 (2022) 5918–5922.
[23] P. Xu, L. Li, R. Li, H. Liu, Dual-circularly polarized spin-decoupled reflectarray with FSS-back for independent operating at Ku-/Ka-bands, IEEE Trans. Antennas Propag. 69 (2021) 7041–7046.
[24] H. Xu, et al., Single-fed dual-circularly polarized stacked dielectric resonator antenna for K/Ka-band UAV satellite communications, IEEE Trans. Veh. Technol. 71 (2022) 4449–4453.
[25] Y. Zhang, et al., A broadband high-gain circularly polarized wide beam scanning leaky-wave antenna, IEEE Access 8 (2020) 171091–171099.
[26] S.-J. Park, S.-O. Park, LHCP and RHCP substrate integrated waveguide antenna arrays for millimeter-wave applications, IEEE Antennas Wirel. Propag. Lett. 16 (2017) 601–604.
[27] Y. Dong, R. Xu, Y.-H. Yang, S.-G. Zhou, Compact shared-aperture dual-band dual-circularly-polarized waveguide antenna array operating at K/Ka-band, IEEE Trans. Antennas Propag. 71 (2023) 443–449.